Role of the Indian Ocean sea surface temperature in shaping the natural variability in the flow of Nile River

Citation: Siam, Mohamed S., Guiling Wang, Marie-Estelle Demory, and Elfatih A. B. Eltahir. "Role of the Indian Ocean Sea Surface Temperature in Shaping the Natural Variability in the Flow of Nile River." Climate Dynamics 43, no. 3–4 (April 17, 2014): 1011–1023.

As Published: http://dx.doi.org/10.1007/s00382-014-2132-6

Publisher: Springer Berlin Heidelberg

Persistent URL: http://hdl.handle.net/1721.1/107175

Version: Author's final manuscript: final author's manuscript post peer review, without publisher's formatting or copy editing

ROLE OF THE INDIAN OCEAN SEA SURFACE TEMPERATURE IN SHAPING THE NATURAL VARIABILITY IN THE FLOW OF NILE RIVER

Mohamed S. Siam[1]

Ralph M. Parsons Laboratory, Massachusetts Institute of Technology, Cambridge, Massachusetts

Guiling Wang
Department of Civil and Environmental Engineering and Center for Environmental Sciences and Engineering, University of Connecticut, Storrs, Connecticut, USA

Marie-Estelle Demory
National Centre for Atmospheric Science, Department of Meteorology, University of Reading, Reading, UK.

Elfatih A. B. Eltahir
Ralph M. Parsons Laboratory, Massachusetts Institute of Technology, Cambridge, Massachusetts

[1]*Corresponding author address*: Mohamed Siam, Ralph M. Parsons Laboratory, Massachusetts Institute of Technology, 15 Vassar St. Cambridge, MA 02139.
E-mail:msiam@mit.edu

ROLE OF THE INDIAN OCEAN SEA SURFACE TEMPERATURE IN SHAPING THE NATURAL VARIABILITY IN THE FLOW OF NILE RIVER

Abstract

A significant fraction of the inter-annual variability in the Nile River flow is shaped by El Niño Southern Oscillation (ENSO). Here, we investigate a similar role for the Indian Ocean (IO) sea surface temperature (SST) in shaping the inter-annual variability of the Nile river flow. Using observations of global SST distribution and river flow in addition to Atmospheric General Circulation Model sensitivity experiments, we show that North and Middle IO SSTs play a significant intermediate role in the teleconnection between ENSO and the Nile flow. Applying partial coherency analyses, we demonstrate that the connection between North and Middle IO SSTs and Nile flow is strongly coupled to ENSO through ocean-atmosphere interactions. During El Niño events, SST in the North and Middle IO increases in response to the warming in the Tropical Eastern Pacific ocean and forces a Gill-type circulation with enhanced westerly low-level flow over East Africa and the IO. This anomalous low-level flow enhances the low-level divergence of air and moisture away from the Upper Blue Nile (UBN) basin resulting in reduction of rainfall and river flow. SSTs in the South IO also play a significant role in shaping the variability of the Nile flow that is independent from ENSO. A warming over the South IO, generates a cyclonic flow in the boundary layer, which reduces the cross-equatorial meridional transport of air and moisture towards the UBN basin, favoring a reduction in rainfall and river flow. This independence between the roles of ENSO and South IO SSTs allows for development of new combined indices of SSTs to explain the inter-annual variability of the Nile flow. The proposed teleconnections have important implications regarding mechanisms that shape the regional impacts of climate change over the Nile basin.

1. Introduction

The Nile basin covers an area of 2.9×10^6 km^2, which is approximately 10% of the African continent (Fig. 1). It has two main tributaries, the White Nile and the Blue Nile that originate from the equatorial lakes and Ethiopian highlands respectively. The Upper Blue Nile (UBN) basin is the main source of water for the Nile River. It contributes to approximately 60% of the main flow of the Nile (Conway and Hulme, 1993). It extends over an area of 175×10^3 km^2 (7°N-12°5'N, 34°5'E-40°E). The mean annual rainfall over this basin is 1200 mm/year (Conway and Hulme, 1993). Almost 60% of the annual rainfall over the UBN occurs during the summer between July and August and the river flow lags rainfall by about one month with an average annual volume of 46 km^3 based on the record for the period 1961-1990 (ElShamy et al., 2009).

The inter-annual variability in the flow of the Nile river is strongly correlated with El Niño Southern Oscillations (ENSO), its warm phase being associated with a reduced Nile flow. Eltahir (1996) determined that sea surface temperature (SST) anomalies over the tropical Eastern Pacific Ocean could explain 25% of the inter-annual variability of the Nile flow. This high correlation is the basis for forecast models that are used to predict the Nile flow (e.g. Wang and Eltahir, 1999; Eldaw et al., 2003). However, the mechanism behind the teleconnection between the Nile flow and ENSO is not yet fully understood.

The connection between El Niño events and the rainfall over East Africa was investigated in several studies (e.g. Bertlando and Camberlin, 1993; Black et al., 2003). However, a clear distinction must be made between rainfall over the Upper Blue Nile basin (Fig. 1) and rainfall over East Africa, which is mainly along the East coast and Horn of Africa and away from the

Ethiopian highlands. The mechanism that connects rainfall over these regions to ENSO is different from the corresponding mechanism in the UBN basin. The UBN basin has one rainy season period (May to September) during which more than 80% of its rainfall occurs, while along the East coast of Africa, and depending on the location from the equator, the seasonal cycle of rainfall have two rainy seasons (Black et al., 2003; Hastenrath et al., 2011). This pattern in the seasonal cycle is related to the migration of the Intertropical Convergence Zone (ITCZ) across the equator over these regions. In addition, the warm phase of ENSO is positively correlated to rainfall during the short rainy season (October to December) over East Africa (Mutai and Ward, 2000), while it is not correlated to rainfall during the long rainy season in March to June; (Pohl and Camberlin, 2006).

The rainfall over the UBN in (May to September) season, is negatively correlated to ENSO. Rainfall over East Africa and the UBN basin are significantly coupled to the intensity of the Indian monsoon (Camberlin, 1995). During El Niño events, the monsoon circulation is weaker due to the modulation of the Walker circulation and the enhanced subsidence over West Pacific and South Asia (Shukla and Wallace, 1983; Ju and Slingo, 1995; Soman and Slingo, 1997 and Kawamura, 1998). Camberlin (1997) suggested that during strong Indian monsoon seasons, sea level pressure over India decreases significantly, which enhances the pressure gradient between East Africa and India, thus increases the westerly winds that advect moisture from the Congo basin to Ethiopia, Uganda and western Kenya. Amarasekera et al. (1997) also suggested that the reduced Nile flow during El Niño events is due to the enhanced subsidence that suppresses rainfall as a consequence of the increased upwelling over the Eastern Pacific ocean. Giannini et al. (2003) also suggested that a warming of the Indian and Atlantic Oceans leads to a reduction in

rainfall over the Sahel region by enhancing convection over ocean and by decreasing convergence of air over land.

In this paper, we aim: (i) to investigate the connection between the Nile flow and ENSO, and in particular, the role of Indian Ocean SSTs in shaping this teleconnection; (ii) develop new indices, based on SSTs over Eastern Pacific and Indian Oceans, which can improve long-term and mid-term climate prediction of the Nile river flow.

2. Description of Data used in this study

The data used in this study consist of observations of river flow and global SST distribution together with reanalysis products that provide information on the atmospheric circulation.

The longest recorded and most accurate hydrological variable that can be considered in this study is the measured stream flow at Dongola (Fig. 1), which can be used as an index of rainfall over the Upper Blue Nile in Ethiopia. The flow at Dongola includes contributions from both the White and Upper Blue Nile rivers, and is referred hereafter as the Nile flow. However, the signature of the Upper Blue Nile flow on the Nile flow is dominant. The Upper Blue Nile provides more than 60% of the annual mean Nile flow at Dongola. Moreover, more than 80% of the JJASO (June-October) mean Nile flow is a result of the summer rainfall over the Upper Blue Nile. More importantly, the flow in the Blue Nile explains most of the inter-annual variability in the flow of the Nile river. The monthly mean flow data at Dongola were extracted from the Global River Discharge Database (RivDIS v1.1) for the period 1871-2000 (Vörösmarty et al., 1998).

The SST data were extracted from the global monthly mean (HadISST V1.1) dataset, available on a 1-degree latitude-longitude grid from 1871 to 2000 (Rayner et al. 2003). Monthly anomalies of the SSTs were averaged over three Eastern Pacific Ocean regions (2^{o}N-6^{o}N, 170^{o}W-90^{o}W; 6^{o}S-2^{o}N, 180^{o}W-90^{o}W; 10^{o}S-6^{o}S, 150^{o}W-110^{o}W) and used as ENSO indices. These regions have the highest correlations with the mean Nile flow and cover the same areas as the Niño 3 and 3.4 indices (Trenberth, 1997). In addition, monthly anomalies of SSTs were averaged over three different regions in the Indian Ocean (IO). These regions are defined hereafter as the North IO (0-15^{o}N, 50^{o}E-70^{o}E), the Middle IO (10 ^{o}S-0, 50^{o}E-70^{o}E) and the South IO (25^{o}S-35^{o}S, 50^{o}E-80^{o}E). Also, these regions exhibit the highest correlations with the Nile flow, compared to other regions of the IO.

The variables considered to study the atmospheric circulation in response to changes in SST include zonal and meridional wind speed components on pressure levels. These are obtained from the ERA-Interim (ERAI) reanalysis product for the period 1979-2010 (Dee et al., 2011). ERAI was chosen among other reanalysis products because it has the most accurate representation of the hydrological cycle over the UBN basin (Siam et al., 2013) and wind circulation over Africa compared to other reanalysis products such as ERA40 (Uppala et al., 2005) or NCEP-NCAR (Kalnay et al., 1996).

3. Observational Analyses of the relationships between Nile flow and SSTs in Indian and Pacific Oceans

3.1. Cross-correlation analyses

In this section, a detailed analysis of correlations between SSTs over the Indian and Pacific Oceans and the Nile flow is presented. From July to October, tropical Eastern Pacific SSTs show a persistent and significant negative correlation with the JASO (July-October) mean Nile flow for the period (1871-2000) as illustrated in Figs. 2a to 2d. Figs. 3a to 3d show the correlation between SON (September-November) mean ENSO index and the global SST distributions in July, August September, and October. The comparison between Figs. 2 and 3 reveals that the correlation between the Nile flow and the global SSTs seems to reflect the correlation between ENSO and those SSTs. Therefore, the global SSTs in regions other than the East tropical Pacific may not explain any significant additional variability in the Nile River flow. One significant exception is the correlation between JASO mean Nile flow and South IO SSTs in August. This correlation is significant (R^2~0.3) and is not simply a reflection of the significantly smaller correlation (R^2~0.2) between ENSO index and SSTs in the same region of the South IO, and in the same month of August. This result suggests that the South IO may play an independent role from ENSO in shaping the variability of the Nile flow.

In order to estimate the highest correlation between the Nile flow and ENSO, Fig. 4 shows the correlation between the ENSO index, considered separately for each month of the year, and the mean Nile flow over several months of the rainy season (JJAS: June-September, JASO: July-October, ASON: August-November). The JASO mean Nile flow has the highest negative correlation with ENSO index, especially during the months of September to November. This result may be explained as due to the fact that all the Nile flow from July to October is necessary to consider in order to capture all the variability in the rainfall over Ethiopia during the entire rainy season from June to September and the signal of ENSO is the strongest during September to November (Wang and Eltahir, 1999).

The correlation analysis is repeated between the Nile flow averaged for JASO and monthly SSTs averaged over three different regions in the Indian Ocean: North IO, Middle IO, South IO (defined in section 2). The SST is considered separately for each month of the year. The JASO mean Nile flow is negatively correlated with North and Middle IO SSTs from September to December (Fig. 5). This period of high negative correlation lags by approximately one month the high correlation found between the JASO mean Nile flow and monthly ENSO index (blue line of Fig. 4). This lag is consistent with the lag estimated in the cross correlation analysis between the monthly Nile flow and the monthly SSTs in Indian Ocean where the peak of the correlation occurs at a lag of approximately 2 to 3 months while with a similar lag is estimated with the ENSO index of about 2 months as shown in Fig. 6a. The lagged anti-correlation between the Nile flow and the Indian Ocean SSTs compared to ENSO is explained by the fact that North and Mid IO SSTs respond to ENSO (Fig. 6b; Nicholson, 1997; Cole et al, 2013). This lag is consistent with the time required for the warm water to travel from the Pacific to the Indian Ocean through the "Indonesian through flow" and advection by the Indian Equatorial Current (Tomczak and Godfrey, 1995).

The cross-correlation in Fig. 6a should be interpreted with caution. The cross-correlation analysis needs continuous time series, while most of the annual flow in the Nile occurs during the rainy season from June to October. It is unavoidable that the use of the whole monthly flow time series (including the winter season) suppresses the magnitude of the cross-correlation, and results in an apparently lower cross-correlation coefficient. However, these results can still be used to support qualitative reasoning. The peak of the cross-correlation between Nile flow and Indian Ocean SSTs occurs one month later than the corresponding peak between the Nile flow and ENSO. This

result indicates that the North and Middle IO SSTs are strongly linked to ENSO, which reveals that any indices based on the North and Middle IO SST cannot be used independent from the ENSO index to predict the Nile flow. On the other hand, using the whole time series, the SST in the South Indian Ocean shows a low cross-correlation with the Nile flow because significant correlation only occurs during one month in August (Fig. 6a). However, South IO SSTs are significantly less dependent on ENSO. The South Indian Current cools the South IO surface and decreases the effect of the warm South Equatorial Current on the South Indian Ocean (Tomczak and Godfrey, 1995).

3.2. Partial Coherency analysis

The dependence of the Nile flow on SSTs in the Indian and Pacific Oceans is analyzed in this section using partial coherency analysis. “Partial coherency” represents a generalization of the concept of partial correlation coefficient. Partial correlation analysis focuses on the relationship between two variables in the presence of a third variable (Jobson, 1991). It quantifies the correlation between these two variables after evaluating the impact of the third variable. In this study, the two variables are the Nile flow and IO SSTs, and the third variable is the ENSO index. The partial correlation coefficient quantifies how much of the Nile flow variability, which cannot be explained by ENSO, is explained by IO SSTs. However, the partial correlation coefficient does not show how this correlation is distributed over different frequencies. Here, we apply the partial coherency analysis, which describes how the partial correlation is distributed among different frequencies. By “partial coherency”, we mean the cross-coherency between IO SSTs and the portion of the Nile flow variability that cannot be explained by ENSO.

The ENSO spectrum, calculated from monthly anomalies, depicts a peak at a time scale of almost 50 months (about 4 years; Fig. 7a). The squared coherency spectrum, also calculated from monthly anomalies, shows a high coherency between ENSO and North and Middle IO SSTs at the same time scale of 50 months (Fig. 7b). It shows, however, a low coherency between ENSO and South IO SSTs. This result confirms the cross-correlation analysis illustrated in Fig. 6a in which South IO SSTs depends less on ENSO than North and Middle IO SSTs.

To verify that Indian Ocean SSTs cannot explain any additional variability of the Nile flow, we use the partial coherency analysis as described above but this time between the Nile flow and ENSO and IO SSTs. First, we perform 12 linear regressions from January to December between the monthly-mean Nile flow and the monthly-mean ENSO index (u) months earlier, where (u) denotes the possible lag between ENSO and the Nile flow. The linear regressions depend on the time lag (u) according to:

$$R_{new}(i) = a(i) \times E(i-u) + b(i) \qquad (1)$$

R_{new} (i) is the predicted Nile flow for a specific month (i) where i=1 to 12, and E(i-u) is the ENSO index (u) months earlier than month (i). Accordingly, a(i) and b(i) are also functions of (u).

The Nile flow residuals that are not explained by ENSO are estimated by:

$$R(i, j) = R_{obs}(i, j) - R_{new}(i, j) \qquad (2)$$

R_{obs} (i, j) is the observed Nile flow index in month (i) of year (j), R{new}(i, j) is the predicted flow in year (j). The new time series describing the flow residual R(i, j) contains the part of the Nile flow variability that cannot be explained by ENSO. The partial coherency is the squared

coherency between the time series of the residual flow and the Indian Ocean SSTs. Because of the dependence of the flow residual on time lag (u) between the Nile flow and ENSO, the partial coherency also depends on (u), but our results indicate that the partial coherency estimates are not sensitive to the change of the time lag (not shown). Therefore, the difference between the partial coherences for u=-2, -1, 0, 1, 2 is negligible.

Fig. 8 shows the normal and partial coherency spectrum between the Nile flow and Indian Ocean SSTs. The normal coherency between North and Middle IO SSTs and the Nile flow peaks at the time scale of 50 months (solid lines; bottom panels of Fig. 8), which is similar to the squared coherency between ENSO and the Nile flow (top left panel). However, the partial coherency is almost zero at the position of this peak (dashed lines). The normal and partial coherencies between the Nile flow and South IO SSTs are both smaller than the normal coherencies between the Nile flow and North and Middle IO SSTs because the correlation has only one peak in August (Fig. 5). A detailed analysis between the time series of the JASO mean Nile flow and South IO SSTs in August reveals that they are correlated at time scales of 2 and 4 years (not shown). However, the correlation at the time scale of 4 years is dependent on ENSO, while that at 2 years is independent from ENSO.

These results are consistent with two conclusions:

(1) At the 4-year time scale, North and Middle IO SSTs cannot explain variability in the Nile river flow that is not already explained by ENSO. The peak of the normal coherency at the time scale of 4 years can indeed only be explained by a response of North and Middle IO SSTs to ENSO that leads to a response in the Nile flow.

(2) The South IO SSTs explain some of the variability of the Nile river flow that is not explained by ENSO. Hence, the South Indian Ocean is the only region of the IO that plays a role in shaping the variability of the Nile flow that is independent from ENSO.

4. Mechanism relating the Indian Ocean SSTs and UBN flow

It is shown in the previous section that the Nile river flow is moderately correlated with the SSTs in the Indian Ocean. Furthermore, we found that the SSTs in the North and Middle Indian Ocean respond to the warming in the Pacific, while the SSTs of South Indian Ocean are less dependent on the Pacific SSTs. In this section we propose a mechanism that explains these teleconnections between ENSO, Indian Ocean SSTs and Nile flow.

Fig. 9 shows the ERAI averaged wind fluxes at 800 mb during August 1979-2011. The wind circulation is mainly composed of two anticyclones in the North and South of the Equator. The anticyclone located in the South is responsible for maintaining the cross-equatorial meridional southerly flow and the associated convergence of air over the UBN basin. The anticyclone located in the North is associated with low level westerly winds that forces divergence of air away from the UBN.

The intensity of the anticyclonic circulations is reflected in the magnitude of the relative vorticity: strong westerly and cross-equatorial southerly low-level flows correspond to high values of relative vorticity over the North and South Indian Ocean, respectively. It is important to notice that the sign of vorticity in the south of Indian Ocean is positive (anti-clockwise) and negative (clockwise) in the North of Indian Ocean (Fig. 9). The correlation between relative vorticity at 700 mb and convergence of air in the lowest 300 mb over the UBN basin in July is shown on Fig.

10a, and that for August is shown on Fig. 11a. The highest correlation exists over the North Indian Ocean; the positive sign of the correlation indicates that an increase in convergence of air over the UBN is associated with weaker vorticity over North Indian Ocean (i.e. the westerly winds have a smaller magnitude). In addition, a significant positive correlation exist in the South (60^{o}E-80^{o}E, 15^{o}S-25^{o}S) in August, which indicates that the convergence of air over UBN increases when vorticity over this region increases (i.e. cross-equatorial meridional southerly from South Indian Ocean have a higher magnitude).

The magnitude of the relative vorticity over North and South Indian Ocean is negatively correlated with SSTs in both July (Fig. 10b) and August (Fig. 11b). Thus, warming over the Indian Ocean weakens the anti-cyclonic circulation over the South Indian Ocean. On the other hand, warming over the North and Middle Indian Ocean enhances the anticyclonic circulation by inducing westerly winds over the North Indian Ocean. The anomalous westerlies are induced following a Matsuno-Gill circulation forced by an increase in SSTs around the equator, particularly during El Niño years. The Matsuno-Gill circulation pattern responds to an increase in the IO SSTs in July and August (Yang et al., 2007). In addition, the increase of the SSTs over the South of the Indian Ocean, which is independent from ENSO, can similarly generate a cyclonic circulation that enhances the westerly winds over the South Indian Ocean and reduces southerly cross equatorial flow and the corresponding convergence of air towards the UBN basin.

In Figure 12, composite analysis is used to show the difference in winds circulation over the Indian Ocean during warm and cold SSTs conditions for both the NIO and SIO. In this analysis, the HadISST data is used to identify the warm and cold SSTs conditions and ERA-Interim

reanalysis product to provide the corresponding low-level wind circulation. The analysis is limited to the period (1979- 2013) as ERA-Interim is only available during this period. Fig 12a and b show the difference in circulation between the four warmest minus the four coldest SSTs over the NIO and SIO respectively during August. Four events are chosen because they almost represent 10% of the available events (35 events), which makes each analysis include almost 20% of the available data (i.e. 10% warmest and 10% coldest events). Fig. 12a shows the increased westerly winds over the NIO due to the warming of the same region, which reduces the convergence of air of the UBN basin and hence the rainfall. On the other hand, Fig. 12b shows the enhanced cyclonic circulation over the SIO due to warming over that region, which reduces the cross equatorial southerly flow and the associated transport of air and moisture towards the UBN basin and hence reduces the rainfall. These results are consistent with the previous analysis focusing on the relative vorticity and the results in the next section using climate model simulations.

5. Sensitivity experiments on the response of the UBN flow to Indian Ocean SSTs

In order to analyze the mechanism suggested above as well as the connection between the UBN flow and the Indian Ocean SSTs, several sensitivity simulations were performed using the UK Met Office Hadley Centre General Environmental Model version 1 (HadGEM1). Complete description of the model can be found in Johns et al., 2006, Martin et al., 2006 and Ringer et al., 2006. HadGEM1 and its atmospheric version, HadGAM, took part in the Intergovernmental Panel on Climate Change (IPCC) Fourth Assessment Report (AR4) (Solomon et al. 2007). This

model uses hybrid vertical coordinates in height with 38 vertical levels extending to over 39 km and uses a regular longitude-latitude grid at N96 resolution (approximately 135 km at 50N).

We performed four different simulations, in which the SSTs were prescribed for 24 years for the period 1979-2002 using the monthly Atmospheric Model Intercomparison Project II (AMIP-II) sea surface temperature and sea ice (Taylor et al., 2000). The simulations include a control simulation without any changes to the SSTs and three experiments with SSTs during July and August increased by 2^{o}C over the North/Middle, South and both North/Middle and South of the Indian Ocean respectively.

The increased SSTs over the North Indian Ocean mimic, in distribution, the warming that occurs during El Niño events. It is, however, important to note that 2^{o}C is almost four times the standard deviation of the SST variation in these regions. The intention for applying such a large SST warming is to force the model to respond strongly, which makes it easier to analyze the results than with a weak warming. Furthermore, as shown in the previous sections, the SSTs are increased over the South Indian Ocean to show their independent impact from ENSO on the Nile river flow. The monthly mean runoff of the different simulations is shown in Fig. 13. The model was able to simulate the hydrological cycle of the UBN basin by capturing the seasonal cycle of precipitation (not shown) and runoff (Fig. 13). In the control simulation, the magnitude of the annual mean precipitation is 3.53 mm/day, which is close to observations (3.3 mm/day) estimated by the CRU TS3 precipitation dataset (Mitchell and Jones, 2005). Also, the simulated annual mean runoff for the control simulation (0.48 mm/day) represents ~65% of the observed value for the UBN basin (0.76 mm/day). The highest decrease in the annual runoff occurs when the SSTs are increased over both the South and North/Middle of the Indian Ocean (blue line). However, most of the reduction is related to the increased SSTs over the North/Middle of Indian

Ocean (red line). The highest decrease of the runoff is relatively large (i.e. 27 %), relative the coefficient of variation in the observed flow ~22%, which indicates that the UBN flow is sensitive to the warming over selected regions and that SSTs are negatively correlated with the UBN flow. In addition, it is important to notice that we made these experiments with one model; it is possible that other models may have stronger response on the Nile flow for the warming of the Indian Ocean.

The corresponding anomalous wind circulations for the simulation in which the SSTs are increased over the North/Mid and South Indian Ocean are shown in Fig. 14. The anomalous westerlies are seen for August along the coast of Africa and over the North/Middle Indian Ocean following the Matsuno-Gill circulations. These anomalous circulations reduce convergence of air in the boundary layer over the UBN basin and thus the precipitation and the runoff over the basin. The response of the circulation to the warming in the South IO is relatively weak, and fails to reduce the expected impact on the cross-equatorial southerly low-level flow towards the UBN basin. As a result the magnitude of the impact on rainfall and runoff seems low. The mechanism of the teleconnection between the Nile flow and the ENSO and Indian Ocean SSTs is summarized in Fig. 15.

6. Conclusions

In this paper, we investigate the connections between the Nile flow, Indian Ocean SSTs and ENSO. We show that SSTs over North and Middle Indian Ocean are responding to the warming of the Pacific Ocean, particularly during El Niño events. Moreover, they do not force any independent significant variability of the Nile river flow. However, the SSTs over the South of

Indian Ocean are less dependent on ENSO and explain some of the variability of the Nile flow that is not explained by ENSO.

A mechanism that connects the Nile flow to SSTs in Indian Ocean and the Pacific ocean is investigated in this study. The increase of the SSTs over the North and Middle of the Indian Ocean, during El Niño events, forces a Matsuno-Gill circulation over these regions, which enhances westerly winds and reduces the convergence of air over the UBN basin. Similarly the increase in SSTs over the South Indian Ocean generates an anomalous cyclonic circulation that reduces the cross-equatorial southerly low-level flow and the associated convergence of air towards the UBN basin. This reduction in convergence of air is translated to a reduction of rainfall and runoff over the UBN basin. This mechanism was simulated using an AGCM forced with observed SSTs that were modified to simulate a warming over the Indian Ocean. It is shown that increasing SSTs over Indian Ocean reduces the Nile flow, which highlights some of the potential mechanisms shaping the impact of climate change on the Nile river flow, through warming of the Pacific and Indian Oceans.

List of FIGURES

Figure 8: Squared Coherency between the Nile flows and SSTs in the Pacific (ENSO index) and Indian Ocean. The straight dashed lines represent the 1% significance level of the correlation.

Figure 9: Average wind circulation during August (1979-2011) at 800 mb using ERA-Interim reanalysis product. The UBN basin (shaded in brown).

Figure 10: (a) Correlation between the relative vorticity at 700 mb over the Indian Ocean and averaged convergence of air in the lowest 300 mb over the UBN basin (shaded in brown) during July, and b) Correlation between average relative vorticity over (60^{o}E-80^{o}E and 5^{o}S-10^{o}N) and SSTs in the Indian Ocean during July.

Figure 11: (a) Correlation between the relative vorticity at 700 mb over the Indian Ocean and averaged convergence of air in the lowest 300 mb over the UBN basin (shaded in brown) during August and b) Correlation between average relative vorticity over (50^{o}E-70^{o}E and 5^{o}N-10^{o}S) and SSTs in the Indian Ocean during August, and c) Correlation between average relative vorticity over (60^{o}E-80^{o}E and 15^{o}S-25^{o}S) and SSTs in the Indian Ocean during August.

Figure 12: Average winds circulation using ERA-Interim reanalysis for the lowest 300 mb from the surface during August for: a) warm years minus cold years over the NIO, and b) warm years minus cold years over the SIO. The UBN basin is shaded in brown.

Figure 13: Average monthly runoff of the UBN basin (1979-2002) for control simulation compared to three different simulations where the SSTs are increased by 2 ^{o}C over South, North, South and North/Mid of the Indian Ocean. The values between brackets are the percentage reduction relative to the mean annual runoff of the control simulation (0.48 mm/day).

Figure 14: Average wind circulation of August for the lowest 300 mb from the surface and precipitation (1979-2002) for perturbed simulation, where SSTs are increased by 2 ^{o}C over: a) the North/Mid and

South of the Indian Ocean, minus the control simulation, b) North/Mid of the Indian Ocean, minus the control simulation, and c) South of the Indian Ocean, minus the control simulation. The small boxes represent the UBN basin.

Figure 15: Schematic diagram showing the mechanism of the teleconnection between the Nile flow and Indian Ocean SSTs.

REFRENCES

1. Amarasekera, K. N., Lee, R. F., Williams, E. R., and Eltahir, E. A. B: ENSO and the natural variability in the flow of tropical rivers, J. Hydrol., 200, 24–39, 1996.

2. Beltrando, G., and Camberlin, P., 1993: Interannual variability of rainfall in Eastern Horn of Africa and indicators of atmospheric circulation. International Journal of climatology 13, 533-546.

3. Black E., J. Slingo, and K.R. Sperber, 2003: An observational study of the relationship between excessively strong short rains in coastal East Africa and Indian Ocean SST. Mon. Wea. Rev., 31, 74-94.

4. Camberlin P., 1995. June-September rainfall in North-Eastern Africa and atmospheric signals over the tropics: a zonal perspective. International Journal of Climatology 15: 773-783.

5. Camberlin, Pierre, 1997: Rainfall Anomalies in the Source Region of the Nile and Their Connection with the Indian Summer Monsoon. J. Climate, 10, 1380–1392.

6. Conway, D., and M. Hulme, 1993: Recent Fluctuations in precipitation and runoff over the Nile subbasins and their impact on Main Nile discharge. Climatic Change, 25, 127 - 151.

7. Cole, Julia E., et al. "Tropical Pacific forcing of decadal SST variability in the western Indian Ocean over the past two centuries." Science 287.5453 (2000): 617-619.

8. Dee, D. P., and Coauthors, 2011: The ERA-Interim reanalysis: configuration and performance of the data assimilation system. *Q. J. R. Meteorol. Soc.,* **137**, 553-597.

9. El.Shamy, M. E., 2009: Impacts of climate change on Blue Nile flows using bias corrected GCM scenarios. Hydrology and Earth System. Sciences, 13, 551–565.

10. ElDaw, A., J. D. Salas, and L. A. Garcia, 2003: Long Range Forecasting of the Nile River Flows Using Climate Forcing. J. Applied Meteorology, 42:890-904.

11. Eltahir, E. A. B., 1996: ElNino and the natural variability in the flow of the Nile river. Water Resour. Res., 32(1): 131-137.

12. Giannini, A., R. Saravanan, and P. Chang, 2003: Oceanic forcing of Sahel rainfall on interannual to interdecadal time scales. Science, 302, 1027–1030.

13. Hastenrath, Stefan, Dierk Polzin, and Charles Mutai, 2011: Circulation Mechanisms of Kenya Rainfall Anomalies. J. Climate, 24, 404–412.

14. Jobson, J. D.,1991: Applied Multivariate Data Analysis. Volume I: Regression and Experimental Design, pp. 182-185, Springer-Verlag, New York.

15. Ju, J., and J. M. Slingo, 1995: The Asian summer monsoon and ENSO.Quart. J. Roy. Meteor. Soc., 121, 1133–1168

16. Kalnay, E., and Coauthors, 1996: The NCEP/NCAR 40-Year Reanalysis Project. Bull. Amer. Meteor. Soc., 77, 437-471.

17. Kawamura, R., 1998: A possible mechanism of the Asian summer monsoon-ENSO coupling. J. Meteor. Soc. Japan, 76, 1009□1027.

18. Mantua, N.J. and S.R. Hare, 2002: The Pacific Decadal Oscillation. Journal of Oceanography, Vol. 58 (No. 1), pp. 35-44.

19. Mantua, Nathan J., Steven R. Hare, Yuan Zhang, John M. Wallace, Robert C. Francis, 1997: A Pacific Interdecadal Climate Oscillation with Impacts on Salmon Production. Bull. Amer. Meteor. Soc., 78, 1069–1079.

20. Mutai, Charles C., M. Neil Ward, 2000: East African Rainfall and the Tropical Circulation/Convection on Intraseasonal to Interannual Timescales. J. Climate, 13, 3915–3939.

21. Nicholson, Sharon E. "An analysis of the ENSO signal in the tropical Atlantic and western Indian Oceans." International Journal of Climatology 17.4 (1997): 345-375.

22. Pohl B. & P. Camberlin, 2006: Influence of the Madden-Julian Oscillation on East African rainfall. Part I: Intraseasonal variability and regional dependency. Quarterly Journal of the Royal Meteorological Society 132: 2521-2539.

23. Rayner, N. A.; Parker, D. E.; Horton, E. B.: Folland, C. K.; Alexander, L. V.; Rowell, D. P.; Kent, E. C.; Kaplan, A. , 2003: Global analyses of sea surface temperature, sea ice, and night marine air temperature since the late nineteenth century. J. Geophys. Res.Vol. 108, No. D14, 4407.

24. Siam, S., M., Demory, ME., Eltahir E. A. B.: Hydrological cycles over the Congo and Upper Blue Nile basins: Evaluation of General Circulation Models Simulations and Reanalysis Data Products. J. Climate, in press. doi: http://dx.doi.org/10.1175/JCLI-D-12-00404.1

25. Shukla, J., and J. M. Wallace, 1983: Numerical simulation of the atmospheric response to equatorial Pacific sea surface temperature anomalies. J. Atmos. Sci., 40, 1613–1630.
26. Soman, M. K., and J. Slingo, 1997: Sensitivity of the asian summer monsoon to aspects of sea-surface-temperature anomalies in the tropical pacific ocean. Q. J. R. Meteorol. Soc., 123, 309-336.

27. Tomcza, M. and Godfrey, J. S., 1995: Regional Oceangraphy: an introduction. London. Pregamon

28. Trenberth, K. E., 1997: The Definition of El Niño. Bulletin of the American Meteorological Society, 78, 2771-2777

29. Uppala, S. M., and Coauthors, 2005: The ERA-40 re-analysis. Q. J. R. Meteorol. Soc., 131, 2961-3012.

30. Vimont, Daniel J., 2005: The Contribution of the Interannual ENSO Cycle to the Spatial Pattern of Decadal ENSO-Like Variability. J. Climate, 18, 2080–2092.

31. Vörösmarty, C.J., B. Fekete, and B.A. Tucker. 1998. River Discharge Database, Version 1.1 (RivDIS v1.0 supplement). Available through the Institute for the Study of Earth, Oceans, and Space / University of New Hampshire, Durham NH (USA).

32. Wang, G., and Eltahir E. A. B, 1999: Use of ENSO information in Medium and Long Range Forecasting of the Nile Floods. . J. Climate, 12, 1726-1737.

33. Yang, J. L., Q. Y. Liu, S. P. Xie, et al., 2007: Impact of the Indian Ocean SST basin mode on the Asian summer monsoon, Geophys. Res. Lett., 34, L02708, doi:10.1029/2006GL028571.

34. Zhang, Yuan, John M. Wallace, David S. Battisti, 1997: ENSO-like Interdecadal Variability: 1900–93. J. Climate, 10, 1004–1020.

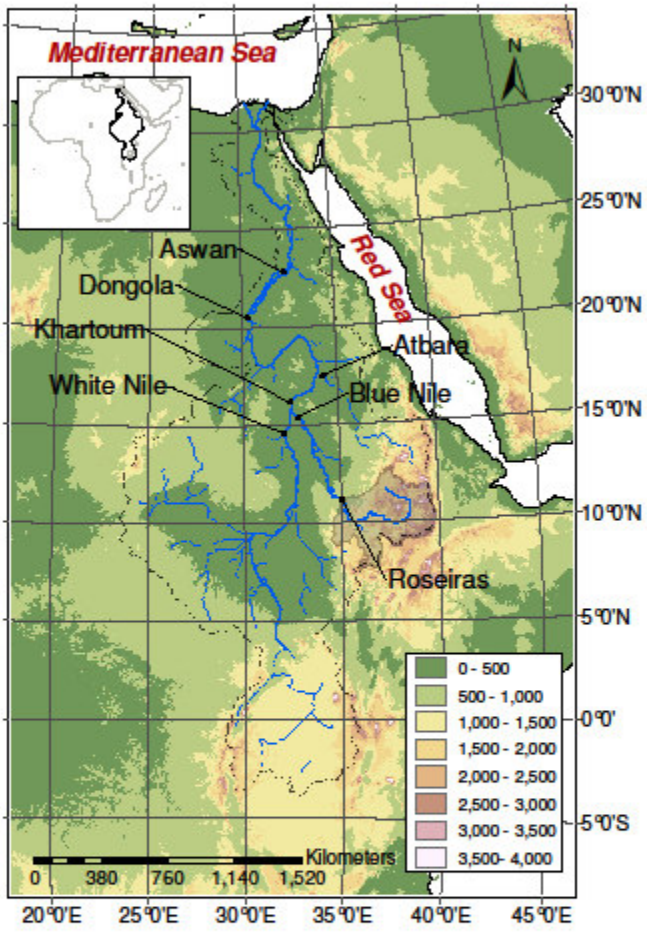

Figure 1: Topographic map of the Nile basin showing the outlet of the Upper Blue Nile basin (shaded in gray) at Roseiras. The White and Blue Nile rivers meet at Khartoum to form the main branch of the Nile river that flows directly to Dongola in the North.

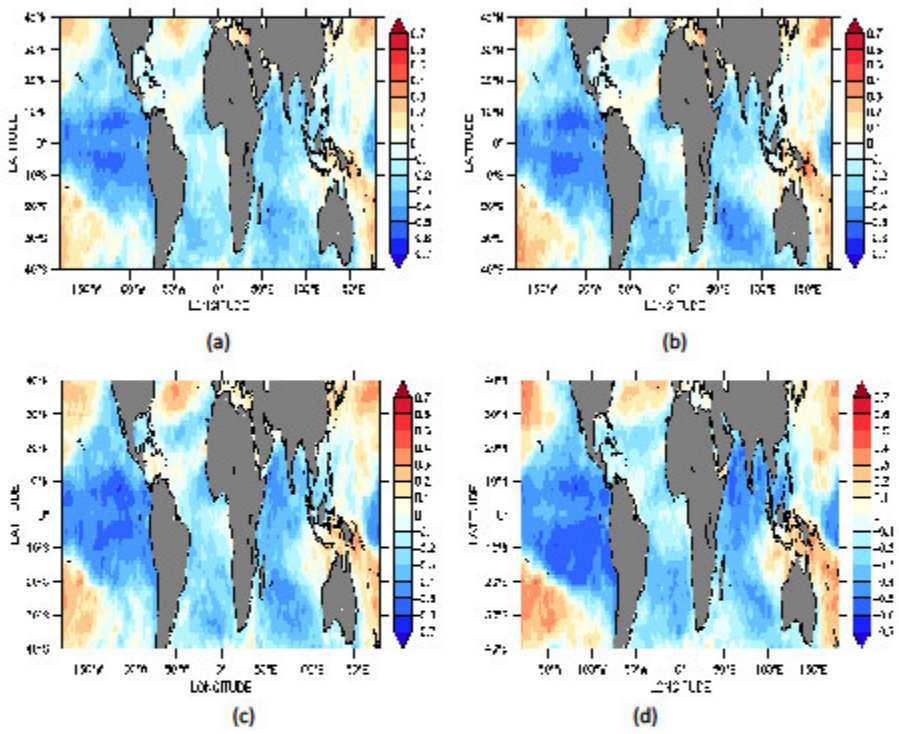

Figure 2: Correlations for the period (1871- 2000) between average Nile flow during (July to October) and average monthly SST: a) July, b) August, c) September and d) October. The 1% significance level of the correlation is 0.23.

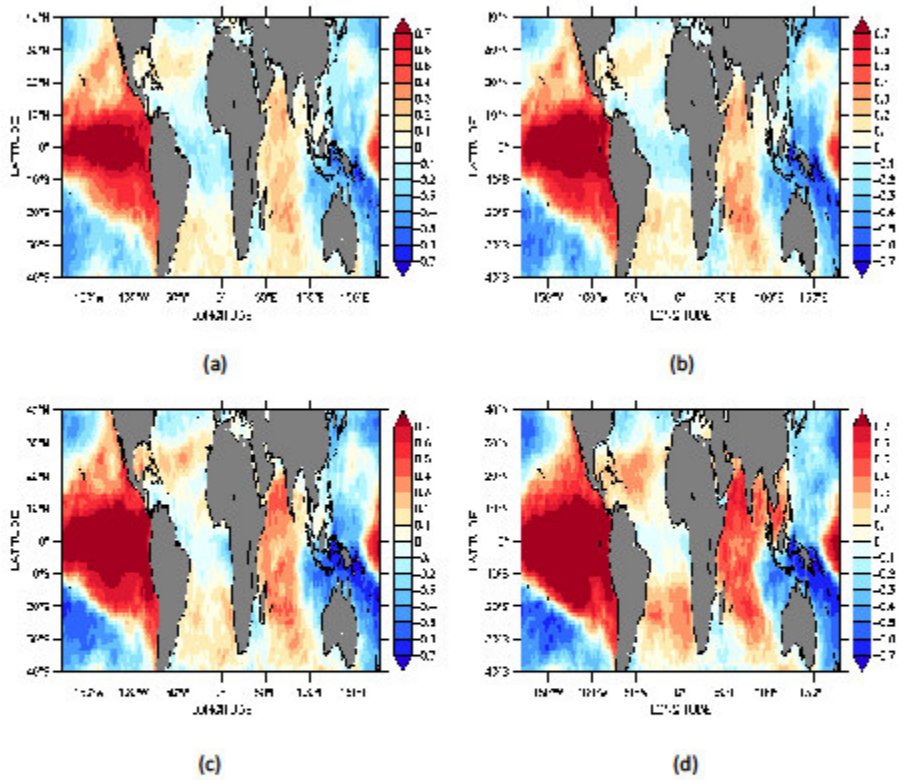

Figure 3: Correlations for the period (1871- 2000) between average ENSO index during (September to November) and average monthly SST: a) July, b) August, c) September and d) October. The 1% significance level of the correlation is 0.23.

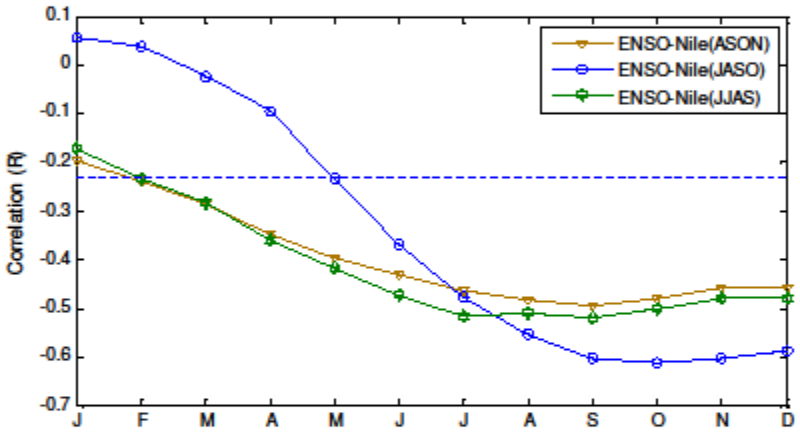

Figure 4: Correlation between the monthly ENSO index and the average Nile flows during July to October (JASO), June to September (JJAS) and August to November (ASON) for 1871 to 2000. The dashed line represents the 1% significance level of the correlation.

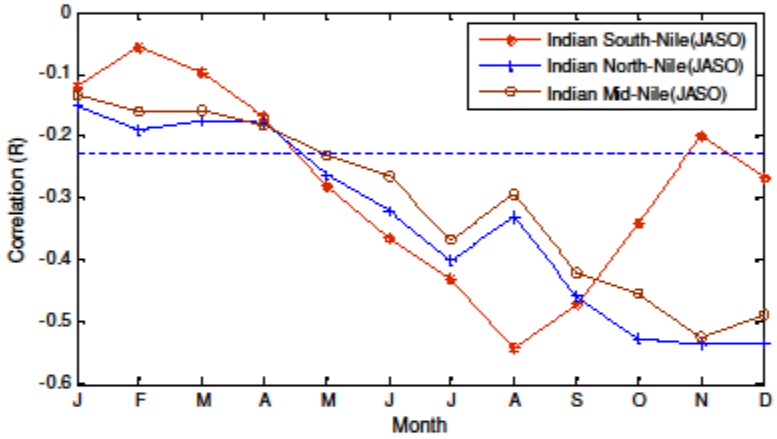

Figure 5: Correlation between the monthly Indian Ocean SSTs and the average Nile flows during July to October (JASO) for 1871 to 2000. The dashed line represents the 1% significance level of the correlation.

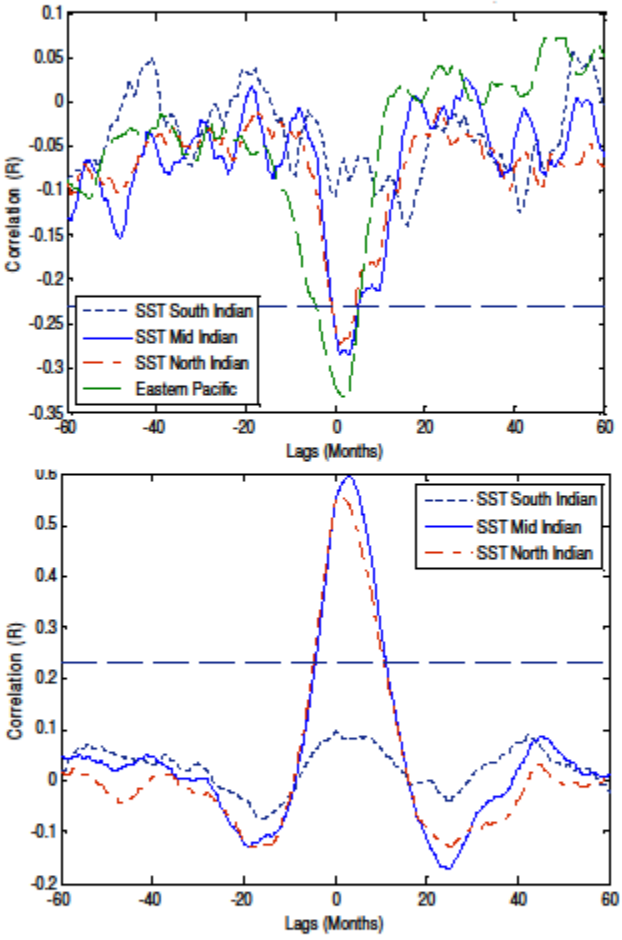

Figure 6: a) Cross Correlation between the monthly SSTs in the three regions of the Indian Ocean and one region in Eastern Pacific Ocean with the monthly Nile flows. b) Cross Correlation between the monthly SSTs in the three different regions of the Indian Ocean and the monthly SST in the Eastern Pacific Ocean for 1871 to 2000. The dashed straight lines represent the 1% significance level of the correlation.

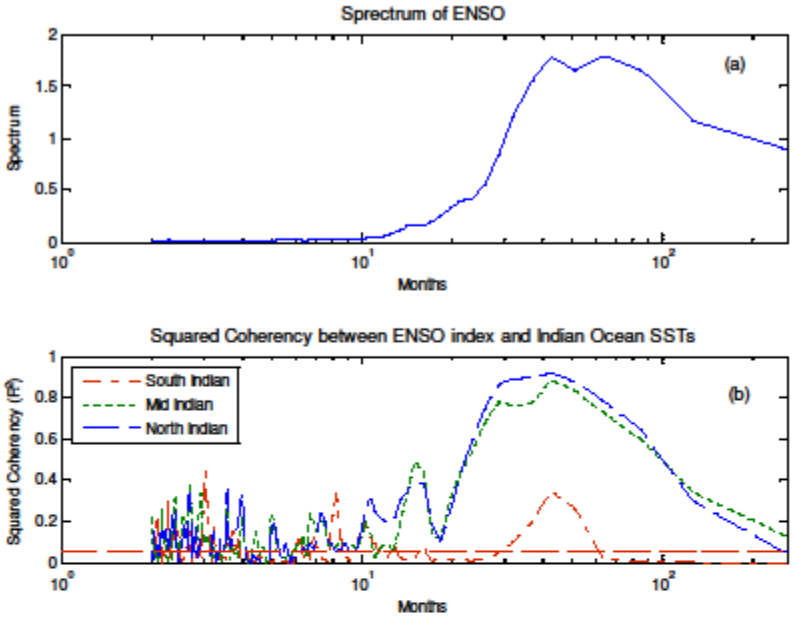

Figure 7: a) Spectrum of ENSO, b) squared coherency between ENSO and SSTS in the Indian Ocean for 1871 to 2000. The straight dashed line represents the 1% significance level of the correlation.

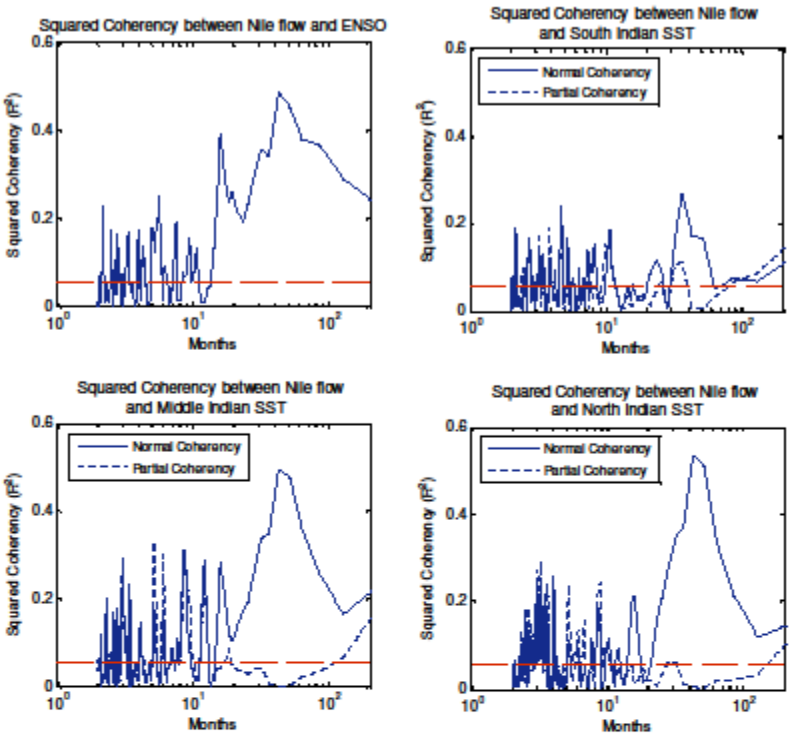

Figure 8: Squared Coherency between the Nile flows and SSTs in the Pacific (ENSO index) and Indian Ocean for 1871 to 2000. The straight dashed lines represent the 1% significance level of the correlation.

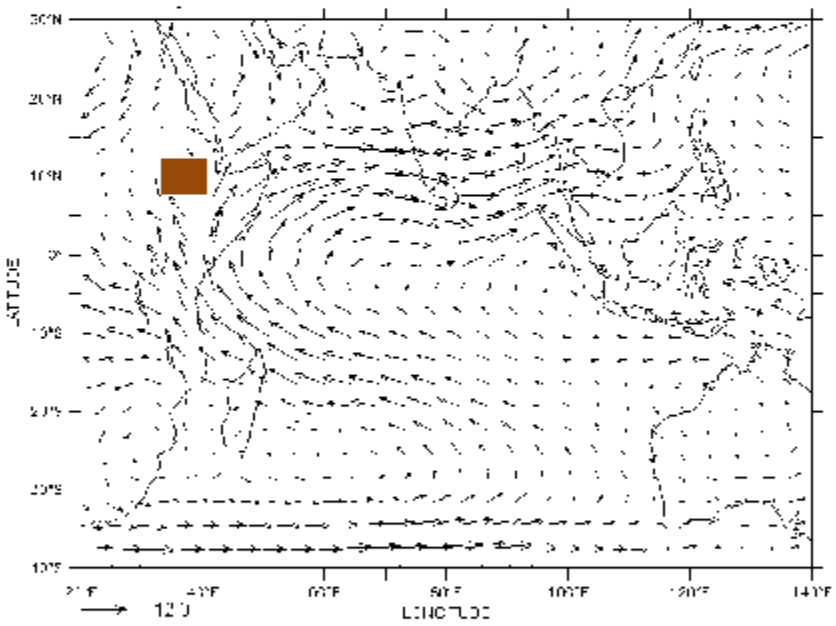

Figure 9: Average wind circulation during August (1979-2011) at 800 mb using ERA-Interim reanalysis product. The UBN basin (shaded in brown).

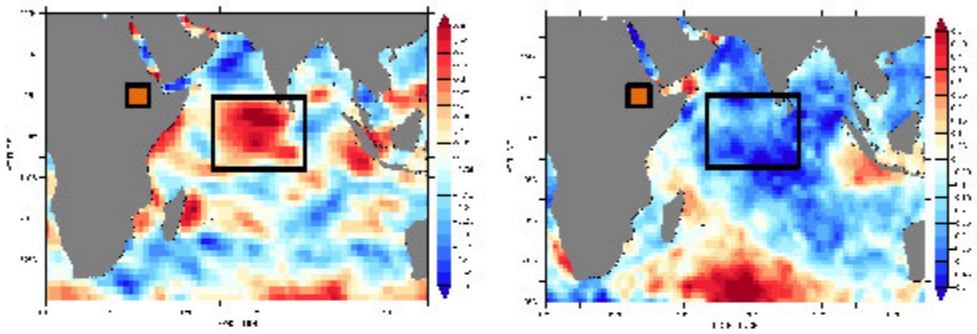

(a) (b)

Figure 10: (a) Correlation between the relative vorticity at 700 mb over the Indian Ocean and averaged convergence of air in the lowest 300 mb over the UBN basin (shaded in brown) during July, and b) Correlation between average relative vorticity over (60°E-80°E and 5°S-10°N) and SSTs in the Indian Ocean during July.

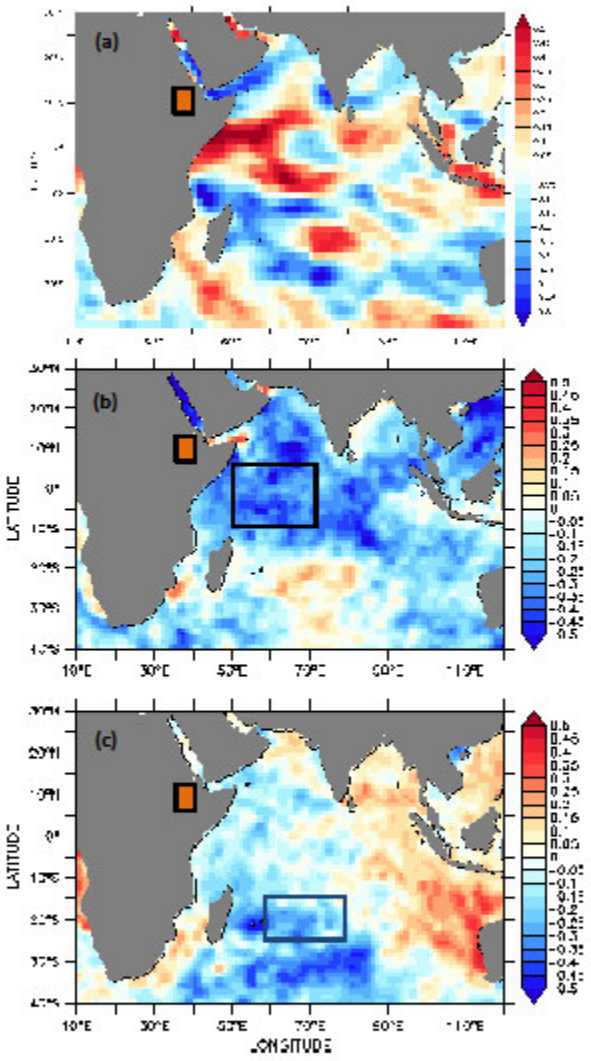

Figure 11: (a) Correlation between the relative vorticity at 700 mb over the Indian Ocean and averaged convergence of air in the lowest 300 mb over the UBN basin (shaded in brown) during August and b) Correlation between average relative vorticity over (50°E-70°E and 5°N-10°S) and SSTs in the Indian Ocean during August, and c) Correlation between average relative vorticity over (60°E-80°E and 15°S-25°S) and SSTs in the Indian Ocean during August.

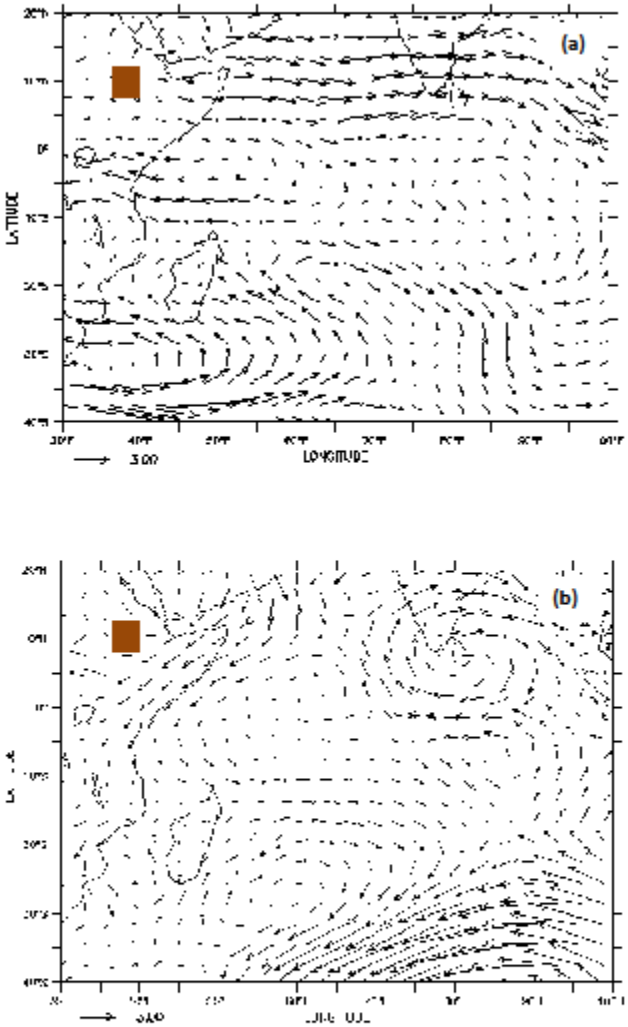

Figure 12: Average winds circulation using ERA-Interim reanalysis for the lowest 300 mb from the surface during August for: a) warm years minus cold years over the NIO, and b) warm years minus cold years over the SIO. The UBN basin is shaded in brown.

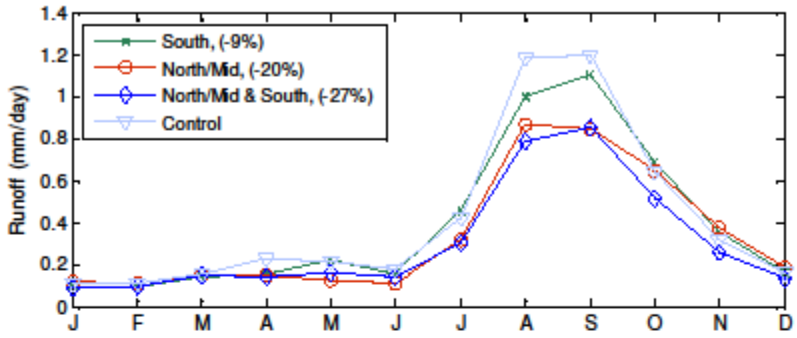

Figure 13: Average monthly runoff of the UBN basin (1979-2002) for control simulation compared to three different simulations where the SSTs are increased by 2 °C over South, North, South and North/Mid of the Indian Ocean. The values between brackets are the percentage reduction relative to the mean annual runoff of the control simulation (0.48 mm/day).

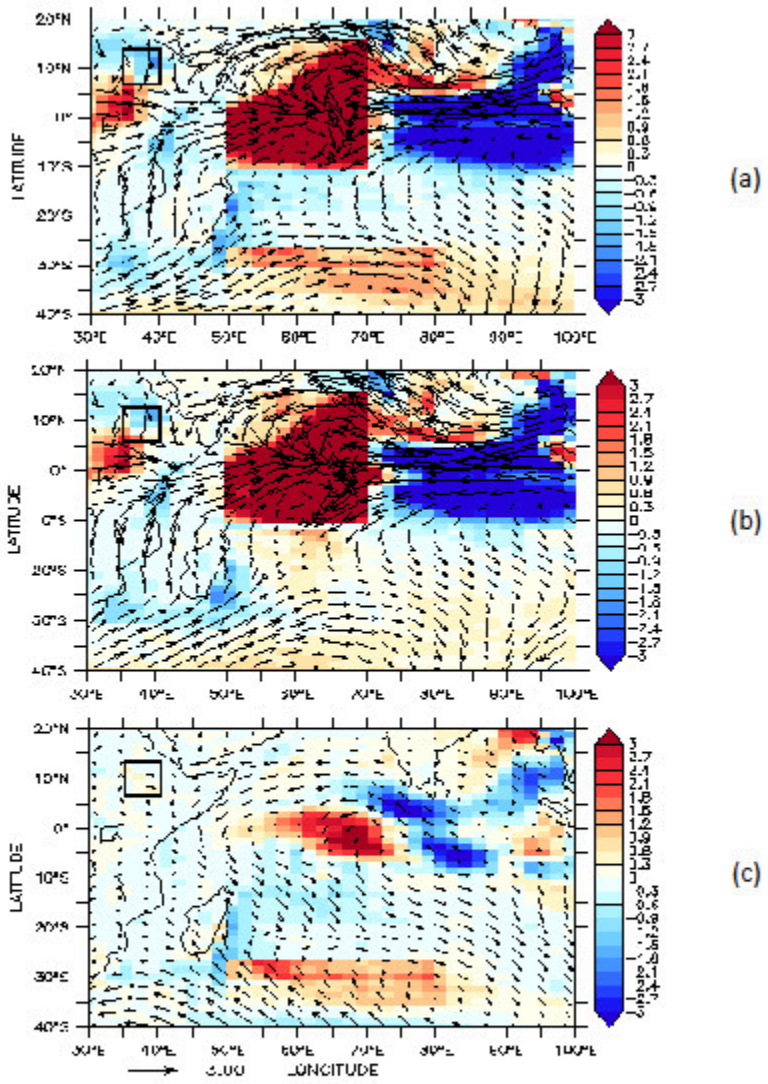

Figure 14: Average wind circulation of August for the lowest 300 mb from the surface and precipitation (1979-2002) for perturbed simulation, where SSTs are increased by 2 °C over: a) the North/Mid and South of the Indian Ocean, minus the control simulation, b) North/Mid of the Indian Ocean, minus the control simulation, and c) South of the Indian Ocean, minus the control simulation. The small boxes represent the UBN basin.

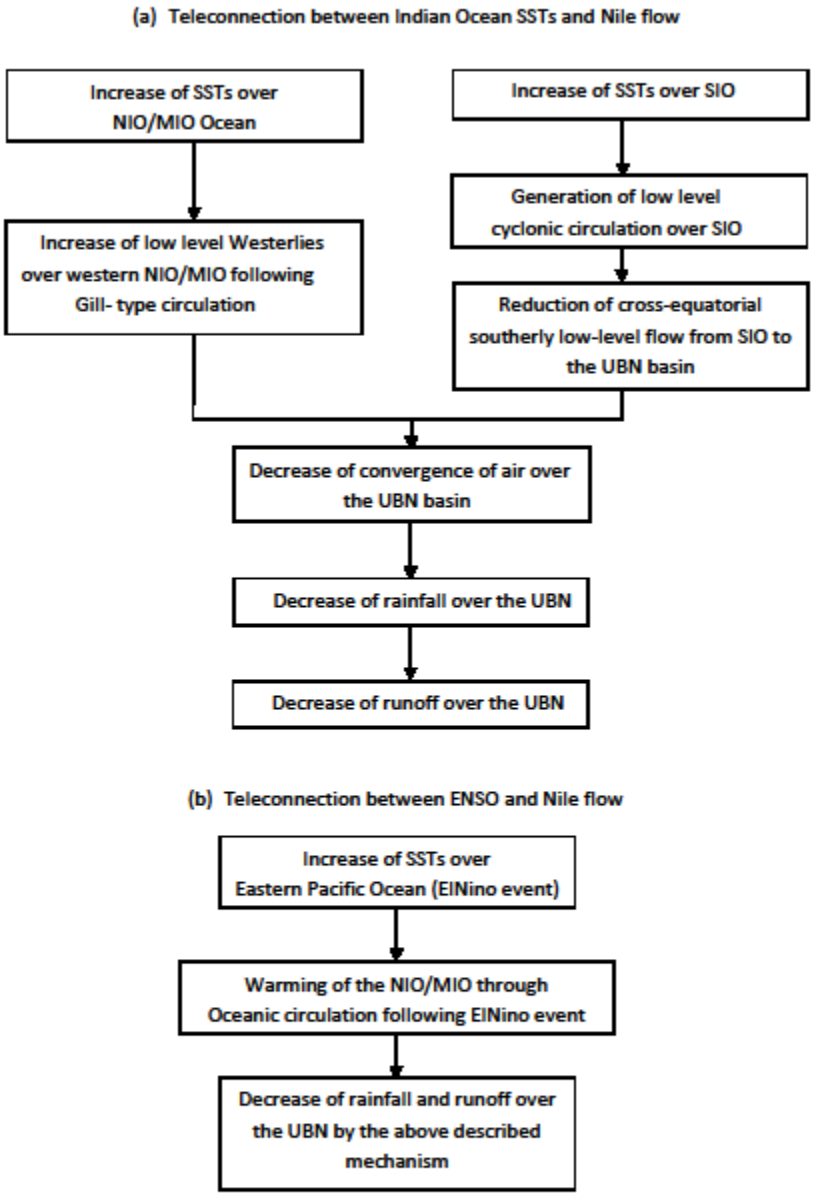

Figure 15: Schematic diagram showing the mechanism of the teleconnection between: a) Indian Ocean SSTs and Nile flow, and b) ENSO and Nile flow.